Original Article

JCBFM

Journal of Cerebral Blood Flow & Metabolism
0(00) 1–13

DOI: 10.1177/0271678X16677990
jcbfm.sagepub.com

SAGE

Brain energy metabolism and neuroinflammation in ageing APP/PS1-21 mice using longitudinal ^{18}F-FDG and ^{18}F-DPA-714 PET imaging

Jatta S Takkinen[1,2], Francisco R López-Picón[1,2], Rana Al Majidi[1,2], Olli Eskola[2], Anna Krzyczmonik[2], Thomas Keller[2], Eliisa Löyttyniemi[3], Olof Solin[2,4,5], Juha O Rinne[6,7] and Merja Haaparanta-Solin[1,2]

Abstract

Preclinical animal model studies of brain energy metabolism and neuroinflammation in Alzheimer's disease have produced conflicting results, hampering both the elucidation of the underlying disease mechanism and the development of effective Alzheimer's disease therapies. Here, we aimed to quantify the relationship between brain energy metabolism and neuroinflammation in the APP/PS1-21 transgenic mouse model of Alzheimer's disease using longitudinal *in vivo* ^{18}F-FDG and ^{18}F-DPA-714) PET imaging and *ex vivo* brain autoradiography. APP/PS1-21 (TG, n = 9) and wild type control mice (WT, n = 9) were studied longitudinally every third month from age 6 to 15 months with ^{18}F-FDG and ^{18}F-DPA-714 with a one-week interval between the scans. Additional TG (n = 52) and WT (n = 29) mice were used for *ex vivo* studies. *In vivo*, the ^{18}F-FDG SUVs were lower and the ^{18}F-DPA-714 binding ratios relative to the cerebellum were higher in the TG mouse cortex and hippocampus than in WT mice at age 12 to 15 months ($p < 0.05$). The *ex vivo* cerebellum binding ratios supported the results of the *in vivo* ^{18}F-DPA-714 studies but not the ^{18}F-FDG studies. This longitudinal PET study demonstrated decreased energy metabolism and increased inflammation in the brains of APP/PS1-21 mice compared to WT mice.

Keywords

Alzheimer's disease, ^{18}F-DPA-714, ^{18}F-FDG, longitudinal imaging, PET

Received 6 July 2016; Revised 7 September 2016; Accepted 12 September 2016

Introduction

The pathophysiology of Alzheimer's disease (AD) has been explained by the amyloid cascade hypothesis, which posits that the accumulation of the amyloid-β (Aβ) peptide in the brain leads to neuronal cell damage and eventually to AD.[1] Increasing knowledge about other pathological mechanisms in AD, such as innate immune-mediated neuroinflammation and deficits in brain energy metabolism and neurotransmitter systems, has led to new ways of thinking about AD progression.[2–5] The development of positron emission tomography (PET) tracers that can measure and monitor biological events in living subjects during disease progression has provided a noninvasive way to study AD *in vivo*.

The use of 2-^{18}F-fluoro-2-deoxy-D-glucose (^{18}F-FDG) PET imaging makes it possible to monitor

[1]MediCity Research Laboratory, University of Turku, Turku, Finland
[2]Turku PET Centre, University of Turku, Turku, Finland
[3]The Department of Biostatistics, University of Turku, Turku, Finland
[4]Turku PET Centre, Åbo Akademi University, Turku, Finland
[5]Department of Chemistry, University of Turku, Turku, Finland
[6]Turku PET Centre, Turku University Hospital, Turku, Finland
[7]Division of Clinical Neurosciences, Turku University Hospital, Turku, Finland

Corresponding author:
Merja Haaparanta-Solin, Turku PET Centre, MediCity Research Laboratory, Tykistökatu 6 A, 20520 Turku, Finland.
Email: mehaaso@utu.fi

changes in glucose metabolism over time in living systems. In AD patients, typical ^{18}F-FDG PET findings include hypometabolism in the parietotemporal cortices, posterior cingulate cortex and the precuneus.[6–8] A decrease in the cerebral metabolic rate of glucose in AD is associated with synaptic activity deficits in the brain. In transgenic (TG) murine models of AD, the use of ^{18}F-FDG PET to investigate alterations in brain energy metabolism in the presence of genetically modified Aβ pathology have produced unclear results. Specifically, different TG mouse models of amyloidosis have shown both increased[9,10] and decreased[11,12] brain energy metabolism. Moreover, the age of the animals and the methodological protocols have not been consistent across the studies.

Neuroinflammation is suspected to be one of the most important factors for promoting cognitive decline in AD,[13] and microglial activation is the main pathological event that leads to neuroinflammation. Microglia are macrophages in the central nervous system that normally help maintain neuronal circuit plasticity and help protect the synapses.[14] When microglia are activated by pathological triggers, they migrate to the site of the injury and initiate an innate immune response. The activation of microglia leads to increased expression of the mitochondrial 18-kDa translocator protein (TSPO), which is associated with AD pathogenesis and which has been used as a target for the development of *in vivo* PET imaging ligands for neuroinflammation.[3,15–18] In recent years, ^{18}F-*N,N*-diethyl-2-(2-[4-(2-fluoroethoxy)phenyl]-5,7-dimethylpyrazolo[1,5-α]pyrimidine-3-yl)acetamide (^{18}F-DPA-714) has been identified as a selective TSPO ligand with demonstrated good binding potential and bioavailability. According to several animal studies, ^{18}F-DPA-714 is better for PET imaging than ^{11}C-PK11195 because of its low nonspecific binding in the brain and its longer half-life.[19,20] Unfortunately, the results of human ^{18}F-DPA-714 PET studies have been conflicting.[21,22] In addition, genetic polymorphism leads to high, mixed or low affinity TSPO binders in human subjects, and this needs to be taken into account when planning a TSPO PET imaging study.[22,23]

It is important to evaluate the use of *in vivo* ^{18}F-FDG and ^{18}F-DPA-714 binding in AD murine models in order to optimise future clinical imaging studies and to develop pharmacological approaches that target both neuroinflammation and energy metabolism. Longitudinal *in vivo* PET studies conducted in suitable AD animal models using radiotracers may help prevent or delay AD by increasing our understanding and awareness of the pathological events that occur in the brain during the course of the disease. Such approaches could also be used to monitor the effects of various interventions. The timing, the origins and the relationships of the pathological changes in AD remain unknown; thus, there is an urgent need for studies that use suitable PET tracers in relevant animal models. In addition, TG murine models that overexpress AD-related genes, such as the human amyloid precursor protein (APP) and presenilin 1 (PSEN1), commonly show only some of the pathological changes observed in patients with AD, not the full spectra.[24] Thus, even refined AD animal models merit further evaluation.

In order to fulfil this demand, we aimed to quantify the relationship between brain energy metabolism and neuroinflammation in the APP/PS1-21 TG mouse model of AD using longitudinal *in vivo* ^{18}F-FDG and ^{18}F-DPA-714 PET imaging and *ex vivo* digital autoradiography. This is the first longitudinal PET imaging study of alterations in cerebral glucose metabolism and neuroinflammation in AD in which the pathological events have been monitored in the same ageing animals over time.

Materials and methods

Radiochemistry

^{18}F-FDG and ^{18}F-DPA-714 were synthesised at the Radiopharmaceutical Chemistry Laboratory at the Turku PET Centre. ^{18}F-FDG was produced from mannosyl triflate with the FASTlab synthesizer (GE Healthcare, Waukesha, WI, USA). The radionuclide labelling was conducted via the nucleophilic substitution reaction as described previously with slight modifications.[25] The radiochemical purity of ^{18}F-FDG exceeded 98%, and the specific activity at the end of the radiosynthesis process was >100 GBq/μmol. ^{18}F-DPA-714 was synthesised according to the original synthesis method.[18] The radiochemical purity of ^{18}F-DPA-714 always exceeded 99.5%, and the specific activity of the ^{18}F-DPA-714 was >1 TBq/μmol.

Animals

All animal experiments were approved by the Regional State Administrative Agency for Southern Finland (permissions ESAVI/4499/04.10.07/2015 and ESAVI/3899/04.10.07/2013) and animal care complied with the guidelines of the International Council of Laboratory Animal Science (ICLAS). In addition, this study was performed in strict compliance with the ARRIVE guidelines, and met the principles of the 3Rs (Replacement, Reduction and Refinement) by using longitudinal PET imaging to examine the same animals repeatedly.

APP/PS1-21 mice (C57BL/6J–TgN(Thy1–$APP_{KM670/671NL}$; Thy1–$PS1_{L166P}$) were originally

provided by Koesler (Rottenburg, Germany) and were further bred in the Animal Centre of University of Turku with C57BL/6Cn mice. APP/PS1-21 mice co-express human APP with the Swedish double mutation KM670/671NL and the L166P mutated human PS1 under the control of a neuron-specific murine Thy-1 gene fragment in a C57BL/6J background.[26] Because of the mutations, Aβ plaques start to develop when the mice are 2 months old, and the plaques are accompanied by microglia proliferation, neuronal degeneration and cognitive decline.[26,27] The animals were housed in individual-ventilated cages, under consistent temperature (21°C ± 1.2°C) and humidity (55% ± 5%) conditions with a 12-h light/dark cycle. They had free access to tap water and certified standard laboratory chow *ad libitum*. Their body weight was measured once at the beginning of every experiment (Figure S1).

Blood glucose and temperature measurements

The body temperature and the blood glucose values of the mice were measured before and after every ^{18}F-FDG injection in the *in vivo* PET and in the *ex vivo* studies. A drop of blood was taken from a tail vein and analysed using Accu-Chek Aviva Nano (Roche Diagnostics, USA), and rectal body temperature was measured with the Physitemp model BAT-12 microprobe thermometer (Physitemp Instruments Inc., NJ, USA).

PET imaging

PET imaging studies were conducted longitudinally using two female and seven male APP/PS1-21 mice (TG, $n_{TOTAL} = 9$), and two male and seven female wild-type control littermates (WT, $n_{TOTAL} = 9$). The mice underwent PET scans at age 6, 9, 12 and 15 months with the Inveon Multimodality PET/CT scanner (Siemens Medical Solutions, Knoxville, TN, USA). The mice were first studied with ^{18}F-FDG, and, after a one-week interval, with ^{18}F-DPA-714.

The *in vivo* study design is presented in Figure S2. Briefly, before each ^{18}F-FDG scan, the mice fasted while placed on a temperature-controlled heating pad for 90 min and were anaesthetised with a 2.5% isoflurane/oxygen mixture 30 min prior to injection. CT transmission scans were acquired for attenuation correction for the PET scans to obtain anatomical reference images. Intravenous bolus injection of ^{18}F-FDG (7.95 ± 0.46 MBq) and 60-min dynamic three-dimensional PET list mode scans with an energy window of 350–650 keV were performed in tandem. The PET list mode data were reconstructed using a two-dimensionally filtered back projection algorithm and Fourier-rebinned into two-dimensional sinograms (51 frames: 30 × 10, 15 × 60, 4 × 300 and 2 × 600 s). The mice recovered after each PET scan for 1 h on the heating pad inside their own cage, and their health was monitored by the researcher.

The ^{18}F-DPA-714 (5.23 ± 1.19 MBq) PET studies followed the same protocol used for the ^{18}F-FDG except for the fast and the measurements of body temperature and blood glucose.

Analysis of PET imaging data

PET imaging data were analysed using Inveon Research Workplace Image Analysis software v. 4.1 (Siemens Medical Solutions). PET/CT images were coregistered with a representative three-dimensional mouse MRI template.[28] Brain uptake of ^{18}F-FDG and ^{18}F-DPA-714 was analysed with volumes of interest (VOIs) drawn over the whole brain, including the olfactory bulbs, cortex, frontal cortex (FC), parietotemporal cortex (PTC), hippocampus (HIPPO), striatum (STR), thalamus (THA), hypothalamus (HYPO) and cerebellum (CB). VOIs were drawn into the CT images by uploading brain region-specific VOI templates into the analysis software. The size of each VOI template was adjusted according to the brain size of every animal. The size of each VOI was approximately 8 mm^3 except for the HYPO VOI (5 mm^3). The mean radioactivity concentrations were evaluated as standard uptake values (SUVs) for ^{18}F-FDG for 30 to 60 min, and the ratios of ^{18}F-DPA-714 binding relative to the CB were evaluated for 30 to 50 min as the time-activity curves plateaued.

Ex vivo brain autoradiography

Additional TG mice (n = 52; 21 females) and WT mice (n = 29; 14 females) were used for the *ex vivo* digital autoradiography studies. The *ex vivo* ^{18}F-FDG studies were conducted using 6-, 9-, 12- and 15-month-old TG mice ($n_{TOTAL} = 17$; 9 females) and 6-, 9-, 12- and 15-month-old WT mice ($n_{TOTAL} = 19$; 7 females). The *ex vivo* ^{18}F-DPA-714 studies were performed with 1-, 3-, 5-, 10-, 12- and 15-month-old TG mice ($n_{TOTAL} = 35$; 12 females) and 2- and 15-month-old WT mice ($n_{TOTAL} = 10$; 7 females).

The *ex vivo* study design is shown in Figure S3. Briefly, mice fasted for 90 min while placed on a heating pad and were anaesthetised with a 2.5% isoflurane/oxygen mixture for 30 min before ^{18}F-FDG injection. ^{18}F-FDG (7.96 ± 0.35 MBq) was injected intravenously into the tail vein, and each mouse was kept under anaesthesia on the heating pad for 60 min. When the uptake period was over, the mice were sacrificed via cardiac puncture under increased anaesthesia (4.0% isoflurane/oxygen). Transcardial perfusion with

saline was conducted rapidly in order to eliminate blood from the brain. The *ex vivo* ^{18}F-DPA-714 studies followed the same study protocol as the *ex vivo* ^{18}F-FDG studies (Figure S3) except for the fasting and the measurements of body temperature and blood glucose.

After sacrifice, brains were dissected, weighed and the ^{18}F-radioactivity was measured with an automatic γ-counter (Wizard^2, PerkinElmer, Finland). Each brain was frozen with dry ice- (solid CO_2) isopentane. The brains were cut into 20-µm thick coronal cryosections with a CM3050S cryostat (Leica Biosystems, Nussloch, Germany) in the region level of interest as follows: FC (+2.60 mm from the bregma), STR (+1.20 mm from the bregma), anterior hippocampus (ANTH, −1.20 mm from the bregma), posterior hippocampus (POSTH, −2.90 mm from the bregma) and CB (−6.0 mm from the bregma). The cryosections were air-dried and exposed to an imaging plate (Fuji Imaging Plate BAS-TR2025, Fuji Photo Film Co., Japan) for 4 h. The distribution of ^{18}F-radioactivity was exposured to the imaging plate, and the imaging data on the plate were digitised using the BAS5000 analyser (Fujifilm Life Sciences, Japan) with a spatial resolution of 25 µm.

Analysis of digital autoradiography images

The regions of interest (ROIs) were manually drawn on the digital autoradiographs over the FC, PTC, STR, THA, ANTH, POSTH and CB with Aida image analysis software (Image Analyzer v. 4.22; Raytest Isotopenmeßgeräte GmbH, Straubenhardt, Germany). The images were analysed for count densities, which were expressed as background-erased photostimulated luminescence per area (PSL/mm^2). The radioactivity was evaluated for each ROI by comparing the regional brain PSL/mm^2-value to that of the CB.

Immunohistochemistry

The presence of neuroinflammation, plus the amount and the type of the Aβ deposition, were examined by staining the brain sections collected from the *ex vivo* autoradiography studies. Air-dried, fresh-frozen brain sections from different age groups (1- to 15-month-old mice) were post-fixed with 4% paraformaldehyde and stained with thioflavin S (Sigma-Aldrich) or with the antibodies to $A\beta_{1\text{-}42}$ (Millipore Corporation) or iba1 (Wako Pure Chemical Industries, Ltd.). The detailed immunohistochemical staining protocols are described in S4.

Statistics

For the *in vivo* and *ex vivo* studies, the results are expressed as the mean group values ± standard deviation (SD). The statistical analyses were performed with SPSS Statistics v. 23 (IBM) and GraphPad Prism 6.0 software (Graphpad Software). For PET imaging results, the uptake group and the uptake change differences between TG and WT mice during ageing were analysed with repeated measure ANOVA (SPSS v.23). For the *ex vivo* results, the uptake differences and differences in body temperature and blood glucose between TG and WT mice were analysed with the Mann–Whitney U test (GraphPad Prism). The correlation between ^{18}F-FDG and ^{18}F-DPA-714 uptake *in vivo* in TG mice was analysed with the Pearson test (GraphPad Prism), since these results were normally distributed and linear. Differences were considered statistically significant if the p value was less than 0.05.

Results

Longitudinal PET imaging of brain energy metabolism with ^{18}F-FDG

Significantly lower ($p < 0.05$) ^{18}F-FDG $SUVs_{30\text{–}60min}$ were observed in the whole brain, cortex, FC, HIPPO, STR, THA, HYPO and CB of 12-month-old TG mice (n = 9) compared with age-matched WT mice (n = 9). Compared with 15-month-old WT mice, the age-matched group of TG mice showed further decreases in ^{18}F-FDG $SUV_{30\text{–}60min}$ values in the same brain regions ($p < 0.05$), and also in the PTC (Figure 1, Table 1). There was no intergroup difference between 6-month-old TG and WT mice.

There were significant ($p < 0.05$) differences in the mean ^{18}F-FDG uptake changes from 6 to 12 months between TG and WT mice in the whole brain, cortex, FC, PTC, HIPPO and STR (Figure 1, Table S6). Furthermore, there were significant differences in the mean ^{18}F-FDG uptake changes in the whole brain, cortex, FC, PTC, HIPPO, STR, THA, HYPO and CB between TG and WT mice from 6 to 15 months ($p < 0.05$) (Figure 1, Table S6). The differences plateaued rather than increasing further from 12- to 15-month-old mice.

The heating pad used for the PET/CT experiments was broken when the ^{18}F-FDG PET imaging studies were conducted at 9-month time point. All data from the 9-month-old TG and WT mice were excluded from the final analyses in order to have consistent conditions throughout the longitudinal study.

Longitudinal PET imaging of neuroinflammation with ^{18}F-DPA-714

Significantly higher ($p < 0.05$) ^{18}F-DPA-714 $CB_{30\text{–}50min}$ ratios were observed in the cortex, FC, PTC and STR

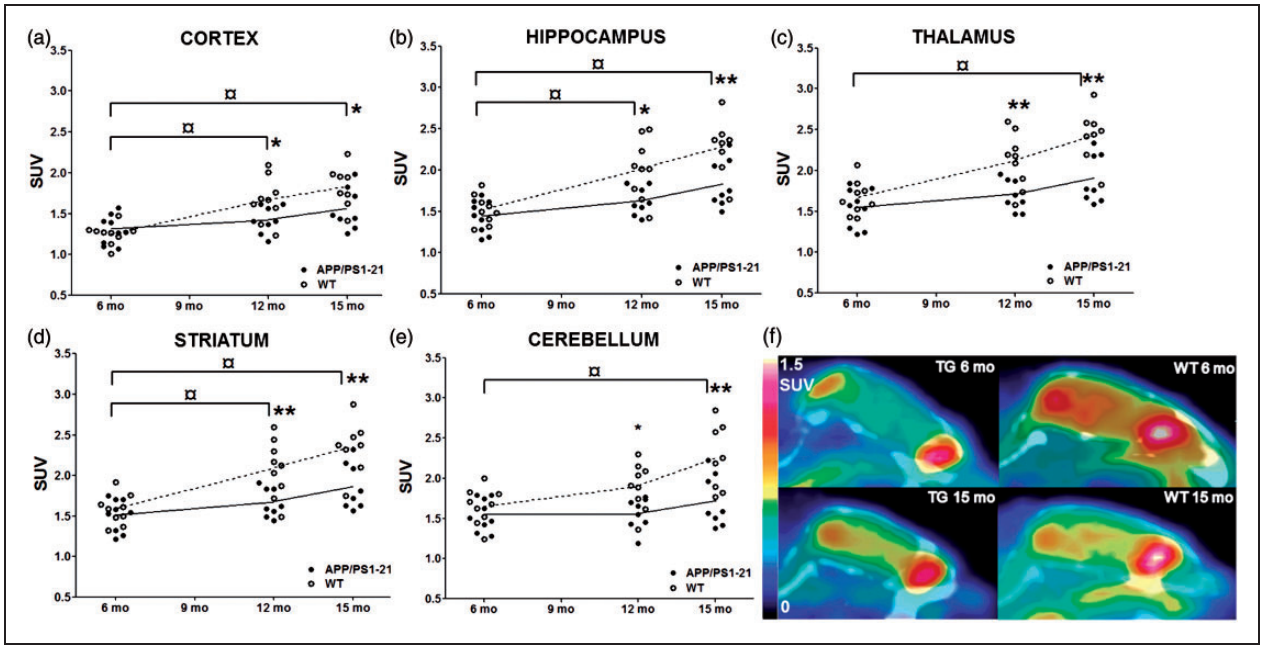

Figure 1. *In vivo* ^{18}F-FDG uptake in APP/PS1-21 TG (n = 9) and WT mice (n = 9) at age of 6, 12 and 15 months, presented as standard uptake values (SUVs) in the (a) cortex, (b) hippocampus, (c) thalamus, (d) striatum and (e) cerebellum. (f) Shows representative sagittal ^{18}F-FDG PET images of an APP/PS1-21 mouse (TG) at age 6 and 15 months (left) and of a WT mouse at age 6 and 15 months (right) (for intergroup differences: $^{*}p < 0.05$, $^{**}p < 0.005$; for mean uptake changes from 6 to 12/15 months: $^{¤}p < 0.05$).

Table 1. *In vivo* ^{18}F-FDG uptake in APP/PS1-21 and WT mice according to age.

	6 months			12 months			15 months		
	TG	WT	*p*	TG	WT	*p*	TG	WT	*p*
Brain	1.42 ± 0.19	1.48 ± 0.17	ns	1.55 ± 0.17	1.91 ± 0.31	**	1.74 ± 0.28	2.16 ± 0.30	**
Cortex	1.30 ± 0.18	1.25 ± 0.13	ns	1.42 ± 0.17	1.67 ± 0.27	*	1.56 ± 0.25	1.83 ± 0.25	*
Frontal cortex (FC)	1.40 ± 0.18	1.35 ± 0.14	ns	1.52 ± 0.18	1.87 ± 0.33	*	1.70 ± 0.31	2.03 ± 0.31	*
Parietotemporal cortex (PTC)	1.30 ± 0.17	1.24 ± 0.13	ns	1.42 ± 0.17	1.61 ± 0.25	ns	1.55 ± 0.24	1.80 ± 0.24	*
Cerebellum (CB)	1.55 ± 0.20	1.65 ± 0.23	ns	1.56 ± 0.20	1.90 ± 0.29	*	1.71 ± 0.32	2.25 ± 0.41	**
Hippocampus (HIPPO)	1.44 ± 0.20	1.52 ± 0.18	ns	1.63 ± 0.17	2.01 ± 0.36	**	1.83 ± 0.29	2.28 ± 0.34	**
Striatum (STR)	1.51 ± 0.21	1.58 ± 0.19	ns	1.66 ± 0.18	2.08 ± 0.35	**	1.86 ± 0.28	2.25 ± 0.33	**
Thalamus (THA)	1.54 ± 0.24	1.66 ± 0.21	ns	1.70 ± 0.19	2.12 ± 0.34	**	1.89 ± 0.30	2.43 ± 0.32	**
Hypothalamus (HYPO)	1.36 ± 0.17	1.50 ± 0.17	ns	1.51 ± 0.15	1.84 ± 0.23	**	1.69 ± 0.26	2.10 ± 0.27	**

Note: Data are expressed as the mean standard uptake values (SUVs) ± standard deviation. Significance differences between age-matched TG and WT mice are shown as follows: ns = not significant, $^{*}p < 0.05$, $^{**}p < 0.005$ and $^{***}p < 0.0005$.

of 6-month-old TG mice (n = 9) compared with age-matched WT mice (n = 9) (Figure 2, Table 2). A similar increase in ^{18}F-DPA-714 binding was detected in the cortex and PTC ($p < 0.05$) when the TG mice were 9 months old, and in the cortex, FC, PTC, HIPPO, STR and THA ($p < 0.05$) when the TG mice were 12 months old. The intergroup differences remained significant between 15-month-old TG and WT mice in the cortex, PTC, HIPPO, STR, THA and the whole brain ($p < 0.05$) (Figure 2, Table 2).

There was a significant difference ($p < 0.05$) in the mean ^{18}F-DPA-714 uptake changes relative to the CB in the THA between the TG and WT mice from age 6 to 15 months and from age 9 to 15 months (Figure 2, Table S7). No differences were detected in the mean changes between TG and WT mice from age 6 to 15 months in other brain regions, except for the FC from 6 to 9 months ($p < 0.05$). In other words, the differences in the mean uptake changes between TG and WT mice did not increase during the longitudinal study because

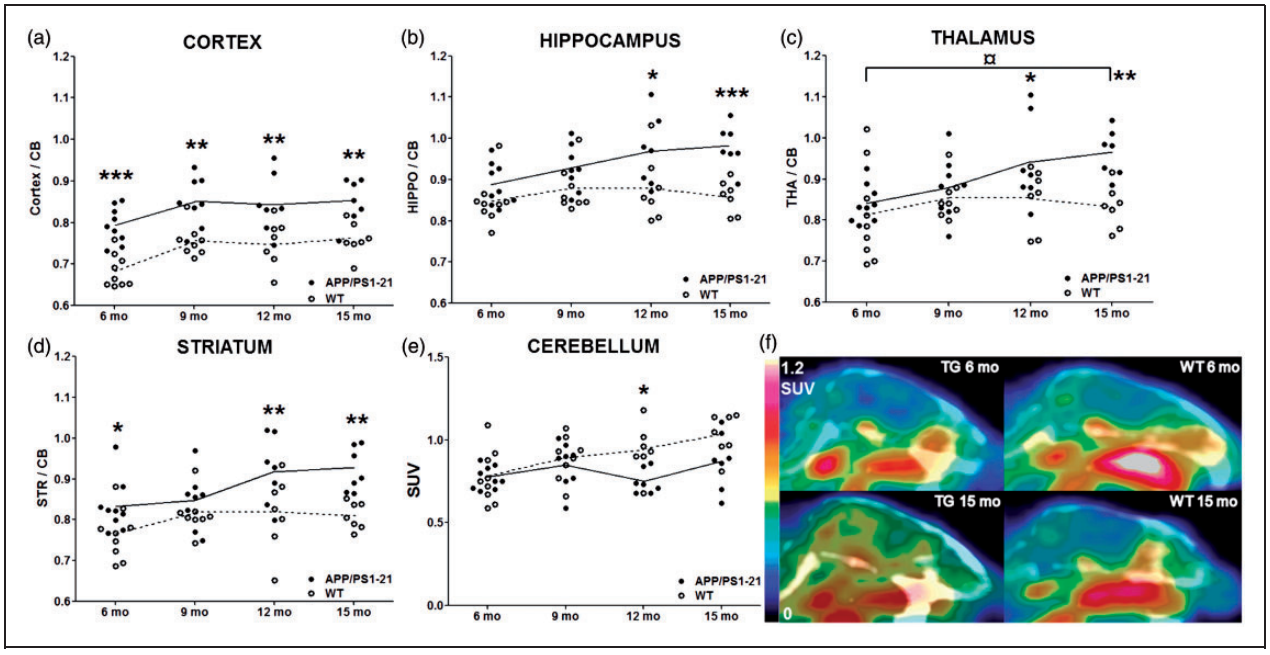

Figure 2. *In vivo* ^{18}F-DPA-714 binding in APP/PS1-21 TG (n = 9) and WT mice (n = 9) at age 6, 9, 12 and 15 months, presented as uptake ratios relative to the cerebellum in the (a) cortex, (b) hippocampus, (c) thalamus and (d) striatum. (e) Shows *in vivo* binding of ^{18}F-DPA-714, presented as standard uptake values (SUVs) in the cerebellum of APP/PS1-21 and WT mice. (f) Shows representative sagittal ^{18}F-DPA-714 PET images of an APP/PS1-21 mouse (TG) at age 6 and 15 months (left) and of a WT mouse at age 6 and 15 months (right) (for intergroup differences: $^{*}p < 0.05$, $^{**}p < 0.005$, $^{***}p < 0.0005$; for mean uptake changes from 6 to 15 months: $^{¤}p < 0.05$).

significant intergroup uptake difference between the TG and WT mice was already reached at the age of 6 months.

Correlation between in vivo ^{18}F-FDG and ^{18}F-DPA-714 uptake in the brain

The correlation between ^{18}F-FDG and ^{18}F-DPA uptake *in vivo* in 6- and 15-month-old TG mice was analysed in the cortex, HIPPO and STR. There was a high positive correlation between the ^{18}F-FDG SUV and the ^{18}F-DPA-714 cortex/CB ($p < 0.005$) and the HIPPO/CB ($p < 0.05$) ratios when TG mice were 6 months old (Table 3). There was a moderate positive correlation between ^{18}F-FDG SUV and ^{18}F-DPA-714 STR/CB (r = 0.636; $p = 0.066$) at the same age. No correlation was observed in 15-month-old mice.

Ex vivo brain autoradiography with ^{18}F-FDG and ^{18}F-DPA-714

Increased region-to-CB-ratios were seen in 12- and 15-month-old TG mice compared with WT mice in the *ex vivo* ^{18}F-FDG autoradiography studies (Figures 3 and 4, and S8). The ^{18}F-FDG FC/CB ratios were significantly higher ($p < 0.05$) in 12-month-old TG mice (n = 3) versus age-matched WT mice (n = 4), but no significant differences were found in other brain regions. The 15-month-old TG mice (n = 4) had significantly higher ($p < 0.05$) region-to-CB-ratios for the FC, PTC and POSTH compared with age-matched WT mice (n = 4) ($p < 0.05$). No differences were observed for the other brain regions in this age group or in younger mice.

In the *ex vivo* ^{18}F-DPA-714 autoradiography studies, increased region-to-CB-ratios were seen in 1-, 3- and 15-month-old TG mice compared with WT mice (Figures 3 and 4, S8, S9). This finding was consistent with the *in vivo* imaging data (Figure 2). The region-to-CB-ratios were significantly higher ($p < 0.05$) in the FC, PTC, POSTH, STR and ANTH of 15-month-old TG mice (n = 5) than in age-matched WT mice (n = 4). Furthermore, the region-to-CB-ratios were higher ($p < 0.05$) in the 1- and 3-month-old TG mice ($n_{1mo} = 6$; $n_{3mo} = 6$) than in the 2-month-old WT mice (n = 6) in the same brain regions as in the 15-month-old mice. There was no difference in the ratios relative to the CB between 2- and 15-month-old WT mice.

Blood glucose values and body temperature of APP/PS1-21 mice

We observed significantly lower ($p < 0.05$) blood glucose values in 12-month-old TG mice than in WT

Table 2. *In vivo* ^{18}F-DPA-714 uptake in APP/PS1-21 and WT mice according to age.

	6 months			9 months			12 months			15 months		
	TG	WT	*p*	TG	WT	*p*	TG	WT	*p*	TG	WT	*p*
Brain	0.93 ± 0.03	0.91 ± 0.05	ns	0.94 ± 0.06	0.94 ± 0.04	ns	0.98 ± 0.07	0.95 ± 0.06	ns	0.98 ± 0.04	0.92 ± 0.02	*
Cortex	0.78 ± 0.04	0.68 ± 0.04	***	0.85 ± 0.06	0.76 ± 0.04	**	0.85 ± 0.07	0.75 ± 0.06	**	0.85 ± 0.05	0.76 ± 0.04	**
Frontal cortex (FC)	0.83 ± 0.04	0.73 ± 0.06	***	0.88 ± 0.08	0.84 ± 0.03	ns	0.88 ± 0.09	0.80 ± 0.07	*	0.90 ± 0.04	0.85 ± 0.06	ns
Parietotemporal cortex (PTC)	0.78 ± 0.05	0.67 ± 0.04	***	0.85 ± 0.07	0.74 ± 0.04	***	0.84 ± 0.08	0.73 ± 0.06	**	0.85 ± 0.07	0.74 ± 0.04	**
Hippocampus (HIPPO)	0.88 ± 0.05	0.85 ± 0.06	ns	0.93 ± 0.06	0.88 ± 0.06	ns	0.97 ± 0.09	0.88 ± 0.08	*	0.98 ± 0.05	0.86 ± 0.04	***
Striatum (STR)	0.82 ± 0.06	0.77 ± 0.06	*	0.85 ± 0.07	0.81 ± 0.05	ns	0.92 ± 0.08	0.82 ± 0.09	**	0.92 ± 0.05	0.81 ± 0.03	**
Thalamus (THA)	0.83 ± 0.05	0.81 ± 0.11	ns	0.88 ± 0.08	0.85 ± 0.05	ns	0.94 ± 0.11	0.85 ± 0.07	*	0.96 ± 0.06	0.83 ± 0.05	**
Hypothalamus (HYPO)	1.31 ± 0.07	1.36 ± 0.17	ns	1.27 ± 0.13	1.34 ± 0.18	ns	1.22 ± 0.22	1.30 ± 0.24	ns	1.20 ± 0.07	1.06 ± 0.12	ns

Note: Data are expressed as the mean radiotracer uptake ratios relative to the cerebellum ± standard deviation. Significance differences between age-matched TG and WT mice are shown as follows: ns = not significant, *$p < 0.05$, **$p < 0.005$ and ***$p < 0.0005$.

Table 3. *In vivo* correlation between brain energy metabolism and neuroinflammation in APP/PS1-21 mice.

	Cortex		Hippocampus		Striatum	
	r	*p* value	r	*p* value	r	*p* value
6 months	0.8619	0.0028	0.8338	0.0052	0.6356	0.0658
15 months	0.0272	0.9538	0.1226	0.7935	0.0480	0.9187

Note: Data are expressed as correlation values (Pearson's r) with *p* values.

mice before the *in vivo* ^{18}F-FDG studies; the values were not significantly different between the two groups at other ages. However, the values tended to be lower in TG mice for every age group compared with age-matched WT mice. The mean body temperatures of the TG and WT mice did not differ either before or after the ^{18}F-FDG injections (Table S5, Figure S5 (a–d)).

Activated microglia and Aβ deposition in the brain

Even at the age of 6 months, APP/PS1-21 mice already had dense Iba1-immunoreactive microglia in the cerebral cortex compared with age-matched WT mice (Figure 4; Figure S8). By the age of 9 months, the abundant microglial cell bodies were bigger, and more activated microglia were observed in other brain regions such as the HIPPO, THA and STR. The amount of Iba1-immunoreactive microglial cells seemed not to increase in TG mice after the age of 9 months.

Thioflavin S staining revealed that the APP/PS1-21 mice had fibrillar Aβ deposits in the cortical areas of the brain at age 6 months, and a few smaller deposits were found in the THA (Figure 4). The amount and the size of Aβ deposits increased from age 6 months to age 9 months in TG mice, and each brain region showed thioflavin S-specific deposits. Similar to the Iba1-findings, the amount of the Aβ deposits seemed not to increase after age 9 months. WT mice had no thioflavin S-specific deposits at any age (Figure S8).

$A\beta_{42}$-driven deposits were investigated using an $A\beta_{42}$ antibody in order to obtain more detailed information about the amyloidosis in these TG mice. Large dense $A\beta_{42}$-specific plaques were abundant in the same brain regions as the Iba1-driven microglia cells, such as the cortex and THA, in 6-month-old TG mice (Figure 4). The $A\beta_{42}$-immunoreactive deposits increased in the TG mice until the age of 9 months and seemed further to increase until the mice were 15 months old. WT mice had no $A\beta_{42}$-specific plaques in the brain (Figure S8).

Discussion

Here, we investigated brain energy metabolism and neuroinflammation in ageing, TG APP/PS1-21 mice

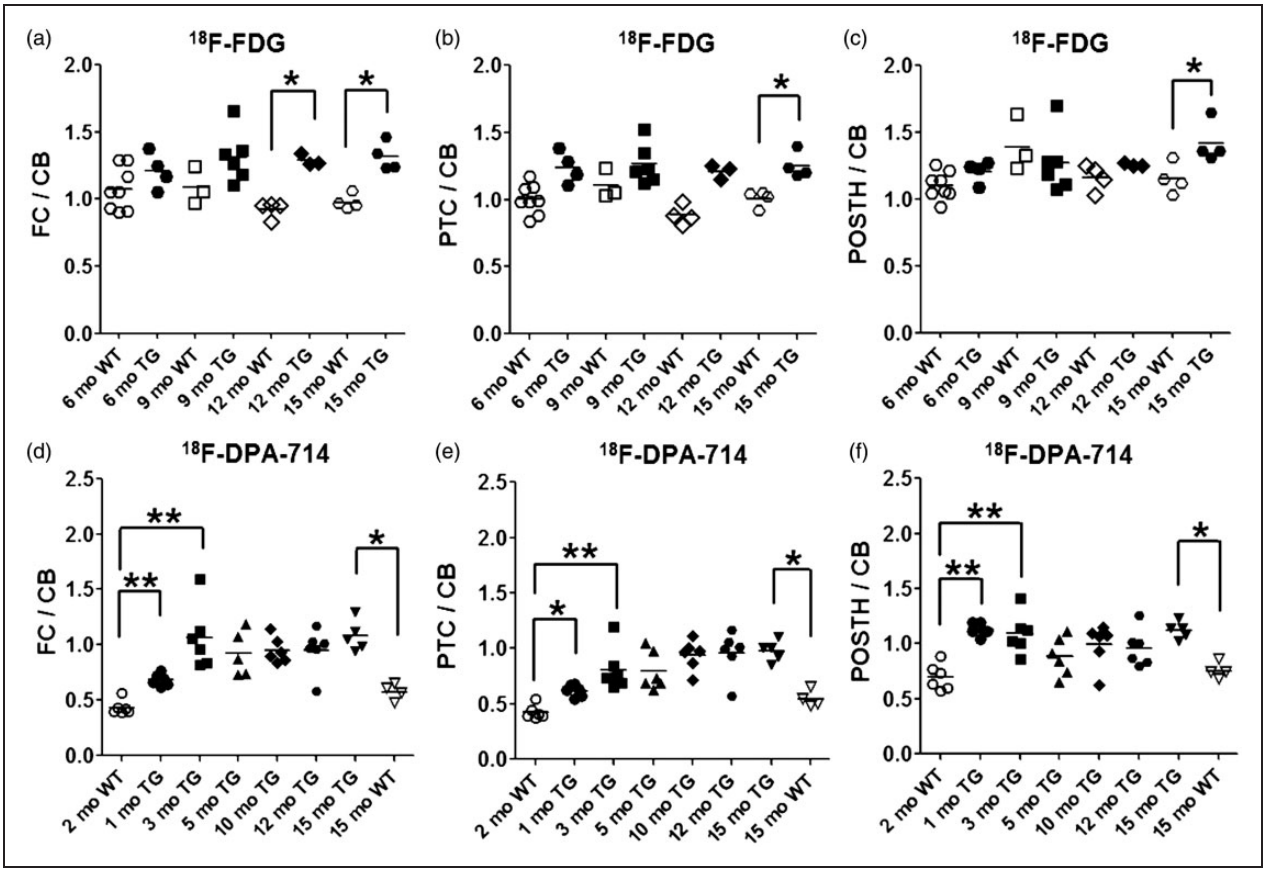

Figure 3. *Ex vivo* brain autoradiography results. ^{18}F-FDG uptake ratios are presented as relative to the cerebellum in the (a) frontal cortex, (b) parietotemporal cortex and (c) posterior hippocampus of APP/PS1-21 TG (n = 17) and WT mice (n = 19) at ages 6 to 15 months. The ^{18}F-DPA-714 binding ratios relative to the cerebellum in the (d) frontal cortex, (e) parietotemporal cortex and (f) posterior hippocampus of APP/PS1-21 TG (n = 35) and WT mice (n = 10) are presented at ages 1 to 15 months (*$p < 0.05$, **$p < 0.005$).

using longitudinal ^{18}F-FDG and ^{18}F-DPA-714 PET imaging.

Brain energy metabolism in APP/PS1-21 mice

Longitudinal PET imaging studies demonstrated that APP/PS1-21 mice exhibited significantly decreased brain glucose utilisation at age 12 and 15 months compared with age-matched WT mice. Significant differences in the mean ^{18}F-FDG changes from 6 to 12 months and from 6 to 15 months demonstrated how TG and WT mice diverge during ageing in terms of glucose utilisation. A plateau phase was not detected from 6 to 15 months, indicating that the glucose utilisation-related pathology continued to increase in TG mice during this time (Figure 1). The *in vivo* results are in line with the PET imaging studies performed in AD patients.[29,30] Not surprisingly, the *ex vivo* results were inconsistent with the *in vivo* data in that they showed increased ^{18}F-FDG binding ratios to the CB in cortical regions and in the HIPPO of 12- and 15-month-old APP/PS1-21 mice. The contrasting binding results are due to the difficulty in finding a reference region, as discussed below.

Previous ^{18}F-FDG studies in other AD mouse models have reported increased or decreased ^{18}F-FDG uptake in TG AD mice versus healthy mice; notably, in AD patients, there is decreased cerebral metabolism in the brain, regardless of the presence of Aβ plaques.[30–33] This decrease in brain glucose metabolism correlates with dementia severity in AD as the disease progresses. In some preclinical animal studies, double TG APP/PS1 ($APP_{K670N/M671L,\ V7171}$ and $PS1_{M146L}$) mouse model, which is commonly used in AD research,[34,35] has exhibited significantly impaired glucose and insulin tolerance at the age of 6 months.[36] In contrast, Poisnel et al. observed in ^{18}F-FDG PET studies that 12-month-old APP/PS1 mice had increased (not impaired) regional cerebral glucose uptake.[9] A single mutation TG Tg2576 ($APP_{K670N/M671L}$) mouse model also showed increased glucose metabolism in 3-month-old animals,[10] whereas PDAPP

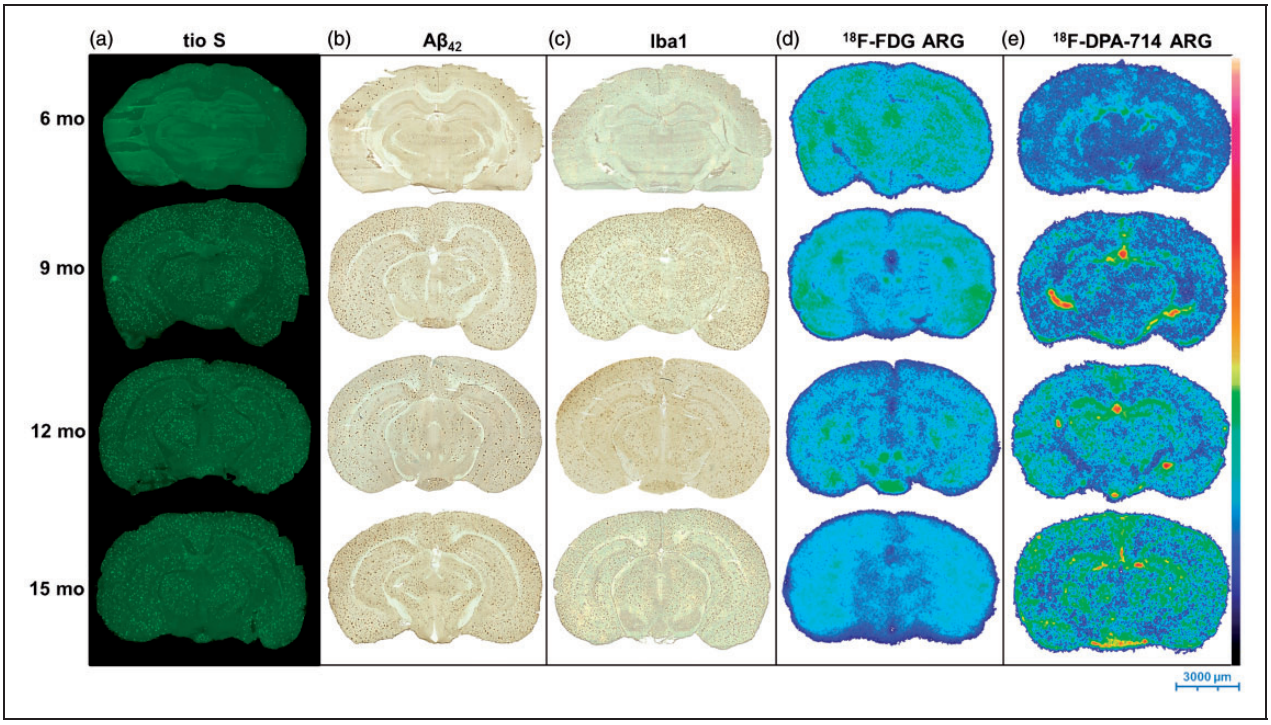

Figure 4. Representative images of brain sections from APP/PS1-21 TG mice are shown at age 6, 9, 12 and 15 months. Immunohistochemical stainings to visualise (a) thioflavin S and (b) $A\beta_{1\text{-}42}$ revealed abundant Aβ depositions in the brain, while (c) Iba1 staining showed activated microglia. Representative *ex vivo* autoradiographs (ARG) of (d) ^{18}F-FDG and (e) ^{18}F-DPA-714 binding in APP/PS1-21 mice, demonstrating the radioactivity of the tracers at 60-min post injection. The ARG figures are individually adjusted in terms of colour.

(APP_{V717F}) mice have shown decreased or increased glucose utilisation in brain ^{14}C-DG autoradiography studies, depending on the brain region and the age of the mice.[11,31] Notably, 12- to 15-month-old 5XFAD ($APP_{K670N/M671L,\ 1716V,\ V7171}$ and $PS1_{M146L,\ L286V}$) mice have also shown varying ^{18}F-FDG uptake results.[37] Macdonald et al. reported that 13-month-old 5XFAD mice, but not younger mice, had significantly lower ^{18}F-FDG uptake, while Rojas et al. have reported elevated ^{18}F-FDG binding ratios relative to the CB in 10-month-old 5XFAD mice.[37,38]

Neuroinflammation in APP/PS1-21 mice

While the TG mice showed age-dependent decreases in ^{18}F-FDG uptake compared with WT mice, there was a significant increase in the mean ^{18}F-DPA-714 uptake in these same TG animals at age 12 and 15 months. The mean changes in ^{18}F-DPA-714 uptake did not change further over time in 6- to 15-month-old mice (or during this interval), except in the THA, showing that the TG and WT mice did not diverge further during ageing in terms of neuroinflammation. This might indicate that neuroinflammation has occurred and indeed reached its peak in the brains of TG mice much earlier than at 6 months of age. However, there were significant intergroup differences between TG and WT mice at 6 months of age in the cortex, HIPPO and STR (Figure 2). Taken together, these data suggest that both aging and Aβ pathology increase brain neuroinflammation in mice, which was shown previously in another APP/PS1 mouse model.[39] Our ^{18}F-DPA-714 autoradiography results were in agreement with our *in vivo* PET data and showed that TG mice had increased uptake ratios relative to the CB for the cortical brain regions and for the HIPPO. Iba1 immunohistochemistry confirmed that there were already abundant activated microglia in the brains of 6-month-old TG mice, and the number of activated cells increased further until the mice were 9 months old.

Our *in vivo* and *ex vivo* data were in line with data from previous preclinical studies of AD. Those studies found that there was microglial activation around the Aβ plaques in TG AD animal models. Similar findings have been reported in *post mortem* brain samples of AD patients, although changes in the immune system and the role of the activated microglia in AD remain a matter of debate.[5,40] In the APP/PS1 animal model, increased neuroinflammation was observed in 16- to 19-month-old mice with ^{11}C-PK11195 PET imaging, and these results were confirmed with Iba1 immunohistochemistry.[41] In younger (13- to 15-month-old) APP/

PS1 mice, ^{11}C-PK11195 PET imaging did not detect neuroinflammation, although Iba1 staining revealed abundant microglia in the brain.[42] Another ^{11}C-labelled tracer, ^{11}C-PBR28, showed increased inflammation in the brains of 6-month-old 5XFAD mice.[43] ^{18}F-labeled TSPO tracers, such as ^{18}F-PBR06, ^{18}F-GE180 and ^{18}F-DPA-714, have been used to detect neuroinflammation in different animal models of amyloidosis: *in vivo* ^{18}F-PBR06 PET imaging differentiated 15- to 16-month-old APP$^{L/S}$ mice from age-matched WT mice,[44] while *in vivo* ^{18}F-GE180 PET differentiated 5- and 16-month-old PS2APP mice[44] and 26-month-old APP/PS1 mice[39] from WT mice. The first and currently the only published longitudinal imaging study to use a TSPO PET tracer was conducted using ^{18}F-DPA-714. In that study, Sérrière et al. repeatedly monitored 6-, 9-, 12-, 15- and 19-month-old APP/PS1 mice using ^{18}F-DPA-714. They only observed increased TSPO tracer uptake in 12- and 19-month-old TG mice compared with their WT littermates.[45] According to previous animal studies, TG mouse models of amyloidosis have demonstrated that microglia decrease Aβ deposits via phagocytosis when the mice are still healthy or during the early stages of AD pathology. When the disease progresses due to the accumulation of Aβ plaques, the microglia are unable to clear the Aβ plaques from the brain.[46–48] This reversal of clearance ability is caused by impaired microglial transitioning and function. As a result, the accumulation of Aβ and the activation of microglia act to stimulate each other, thus accelerating the pathogenesis of AD.[46,49,50]

Analysis of ^{18}F-FDG and ^{18}F-DPA-714 uptake

The spatial resolution of our PET/CT scanner (1.4 mm) affected the quantification of ^{18}F-FDG and ^{18}F-DPA-714 uptake in mouse brain. Therefore, in order to minimise the partial volume effect, we adjusted the size of each VOI relatively large (8 mm^3, HYPO 5 mm^3) and kept it at equal size in each mouse.

SUVs were used to represent the differences in ^{18}F-FDG uptake between TG and WT mice *in vivo*. The SUV is currently the most accepted clinical parameter for measuring glucose utilisation in ^{18}F-FDG PET studies.[51] Our decision to use SUVs was based on our PET imaging results, which detected significantly lower ^{18}F-FDG SUVs in the CB of TG mice versus WT mice, thus revealing pathological alterations in the TG mouse brain. Furthermore, mice gained weight while ageing. Therefore, the only way to compare mice to each other, regardless the age of the animal, was to analyse the uptake results as SUV. Classically, CB has been used as a reference region in preclinical AD ^{18}F-FDG studies,[45] mainly because of the lack of Aβ deposition in the CB of TG animals. However, recent evidence has revealed that AD patients have decreased brain energy metabolism compared with healthy controls, even when there are no Aβ plaques.[30,32,33] Nevertheless, we presented our *ex vivo* data in terms of the region-to-CB ratio because no suitable reference region in tissues other than the brain was observed according to our organ biodistribution studies, which found no uptake differences between TG and WT mice (data not shown). Presenting our *ex vivo* data as the ratios relative to the CB precluded demonstration of hypometabolism in the TG brain. This is, decreased hypometabolism in a target region would not be detected if there was concomitant reduction in the reference region, as shown by our *in vivo* ^{18}F-FDG findings. Deleye et al. discussed a similar phenomenon in their results in which findings of hypometabolism was vanished after calculating the region-to-CB *in vivo*.[31]

We used the CB as the reference region for *in vivo* and in *ex vivo* analyses of ^{18}F-DPA-714 uptake. This decision was based on PET imaging data showing no differences in the ^{18}F-DPA-714 SUV values in the CB between TG and WT mice at any age, except at 12 months, which might have been an anomaly (Figure 2, Tables S10 and S11). In general, there is no true reference region for TSPO, because this protein is found throughout the entire brain, including in the grey and white matter.[52] However, previous studies have suggested that the use of a pseudo-reference region is worthwhile in TSPO imaging research, in order to increase the sensitivity of the PET analysis, as long as there are no differences in SUVs in the reference areas between the study groups.[52] In a recent preclinical AD study, selection of the CB as a pseudo-reference region decreased the intragroup variance in the ^{18}F-GE180 imaging results compared with average SUV analysis.[53] Furthermore, a recent ^{11}C-PBR28 imaging study of AD patients benefited from using the CB as a pseudo-reference region compared with the use of arterial blood input.[52]

^{18}F-FDG study design

The conflicting results from ^{18}F-FDG studies performed in TG murine models of amyloidosis might delay AD research and drug development, because the evaluation of new therapeutic methods relies heavily on preclinical animal studies. There are several reasons why previous studies have failed to demonstrate pathological changes in animal models that are similar to the changes seen in AD patients. First, the chosen single-, double-, triple- or penta-mutation TG AD mouse model used in ^{18}F-FDG studies have different phenotypes that arise from the different mutations.

Second, a wide range of study designs have been used in previous preclinical AD studies, making it difficult to compare the studies.[10,11,38] Third, ^{18}F-FDG PET measures energy utilisation in the whole body, rather than binding to a specific target, and ^{18}F-FDG retention is influenced by many factors. These factors include animal species, genetic modifications, age, temperature, stress, level of alertness, blood glucose level, administration route of ^{18}F-FDG and fasting time. The metabolic rates of mice are almost seven-fold higher than those of humans, and 67% even higher metabolic rates at room temperature (21°C) compared with their normal thermoneutral temperature of 30°C to 34°C. This makes mice more vulnerable to changeable environmental factors.[54–56]

Fasting is used to standardise environmental factors by stabilising the metabolism of the animals and decreasing the endogenous glucose balance in skeletal muscle, brown adipose tissue and cardiac muscle in order to increase the ^{18}F-FDG uptake into the brain.[57,58] However, variations in fasting times in animal studies might affect the results. For example, longer fasting can cause changes in hormonal levels, metabolism and stress levels and even to moderate body weight loss in the animals.[59,60] We used shorter fasting time in our study to realise the benefits of fasting by standardising the metabolic status of the mice, increasing the brain uptake of the tracer and minimising the stress levels of the animals.

Anaesthesia can affect ^{18}F-FDG retention in organs by increasing the endogenous glucose levels.[57,58] In our study, the blood glucose levels did not increase significantly under anaesthesia (Figure S5). We only observed a significant difference in the basal glucose levels between TG and WT mice at 12 months, and these differences may have been due to the genetic mutations in the TG mice. This was observed previously in a different AD model.[31] After consideration of these environmental factors, we performed all of our *in vivo* and *ex vivo* ^{18}F-FDG studies with using isoflurane anaesthesia and a temperature-controlled heating pad and short-term fasting, and we monitored both body temperature and blood glucose levels.

In summary, this is the first longitudinal imaging study in which brain energy metabolism and neuroinflammation were monitored repeatedly over time in the same ageing AD mice. ^{18}F-FDG and ^{18}F-DPA-714 PET imaging showed age-dependent decreases in brain energy metabolism and increases in neuroinflammation in APP/PS1-21 mice. ^{18}F-FDG retention had decreased significantly in 12-month-old TG mice, whereas there was increased ^{18}F-DPA-714 uptake in TG mice relative to WT mice when the study began and the animals were just 6 months old. This finding suggests that neuroinflammation starts much earlier, and this is supported by our *ex vivo* ^{18}F-DPA-714 results from in 3-month-old TG mice. Decline in energy metabolism began much later, when the mice were 12 months old, suggesting the possibility that inflammation-triggered energy metabolism increase begin when the animals are very young.

The high positive correlation between *in vivo* ^{18}F-FDG and ^{18}F-DPA-714 uptake in the 6-month-old TG mice but not in 15-month-old mice demonstrates how energy metabolism decreases while neuroinflammation increases. This phenomenon might be a sign of a compensatory increase in metabolism at disease onset. Accordingly, as the disease progresses, the increase in energy metabolism might vanish.

In conclusion, this study has demonstrated that in a mouse model of AD, Aβ-related pathology is evident at very early stages of life, with different pathological events occurring throughout the course of the disease. The results indicate that translational PET imaging studies are needed to evaluate potential animal models of AD for future preclinical studies on AD drug development. In addition, standard study protocols for ^{18}F-FDG imaging studies should be developed in order to produce AD animal studies on glucose utilisation that can be compared with each other.

Funding

The author(s) disclosed receipt of the following financial support for the research, authorship, and/or publication of this article: Doctoral Programme of Clinical Investigation at the University of Turku; European Community's 7th framework programme (FP7/2007-2013) under grant agreement no. HEALTH-F2-2011-278850 (INMiND); Alfred Kordelin Foundation; Instrumentarium Science Foundation; state research funding from the Hospital District of Southern Finland; and a grant from the Academy of Finland (no. 266891).

Acknowledgements

We thank the staff at the accelerator laboratory and the radiopharmaceutical chemistry laboratory for radionuclide production and tracer analyses, and we thank Elisa Riuttala and Marko Vehmanen in the Medicity Research Laboratory for assistance with the animal experiments.

Declaration of conflicting interests

The author(s) declared no potential conflicts of interest with respect to the research, authorship, and/or publication of this article.

Authors' contributions

MHS, OS, JOR and JST designed the research; AK, OE and TK performed the radiosynthesis; MHS, FRLP, RAM and JST performed the research; EL performed the statistical analysis; JST analysed the data and wrote the paper.

Supplementary material

Supplementary material for this paper can be found at http://jcbfm.sagepub.com/content/by/supplemental-data

References

1. Hardy JA and Higgins GA. Alzheimer's disease: the amyloid cascade hypothesis. *Science* 1992; 256: 184–185.
2. Ferris SH, de Leon MJ, Wolf AP, et al. Positron emission tomography in the study of aging and senile dementia. *Neurobiol Aging* 1980; 1: 127–131.
3. Benavides J, Fage D, Carter C, et al. Peripheral type benzodiazepine binding sites are a sensitive indirect index of neuronal damage. *Brain Res* 1987; 421: 167–172.
4. Bauer J, Strauss S, Schreiter-Gasser U, et al. Interleukin-6 and α2-macroglobulin indicate an acute-phase state in Alzheimer's disease cortices. *FEBS Lett* 1991; 285: 111–114.
5. Heneka MT. Neuroinflammation in Alzheimer's disease. *Lancet Neurol* 2015; 14: 388–405.
6. Minoshima S, Foster NL, Sima AA, et al. Alzheimer's disease versus dementia with Lewy bodies: cerebral metabolic distinction with autopsy confirmation. *Ann Neurol* 2001; 50: 358–365.
7. Mosconi L. Brain glucose metabolism in the early and specific diagnosis of Alzheimer's disease. FDG-PET studies in MCI and AD. *Eur J Nucl Med Mol Imaging* 2005; 32: 486–510.
8. Mosconi L, Tsui WH, Herholz K, et al. Multicenter standardized 18F-FDG PET diagnosis of mild cognitive impairment, Alzheimer's disease, and other dementias. *J Nucl Med* 2008; 49: 390–398.
9. Poisnel G, Hérard AS, El Tannir El Tayara N, et al. Increased regional cerebral glucose uptake in an APP/PS1 model of Alzheimer's disease. *Neurobiol Aging* 2012; 33: 1995–2005.
10. Luo F, Rustay NR, Ebert U, et al. Characterization of 7- and 19-month-old Tg2576 mice using multimodal in vivo imaging: limitations as a translatable model of Alzheimer's disease. *Neurobiol Aging* 2012; 33: 933–944.
11. Valla J, Gonzalez-Lima F and Reiman EM. FDG autoradiography reveals developmental and pathological effects of mutant amyloid in PDAPP transgenic mice. *Int J Dev Neurosci* 2008; 26: 253–258.
12. Nicholson RM, Kusne Y, Nowak LA, et al. Regional cerebral glucose uptake in the 3xTG model of Alzheimer's disease highlights common regional vulnerability across AD mouse models. *Brain Res* 2010; 1347: 179–185.
13. Stefaniak J and O'Brien J. Imaging of neuroinflammation in dementia: a review. *J Neurol Neurosurg Psychiatry* 2015; 0: 1–8.
14. Ji K, Akgul G, Wollmuth LP, et al. Microglia actively regulate the number of functional synapses. *PLoS One* 2013; 8: e56293.
15. Guilarte TR, Kuhlmann AC, O'Callaghan JP, et al. Enhanced expression of peripheral benzodiazepine receptors in trimethyltin-exposed rat brain: a biomarker of neurotoxicity. *Neurotoxicology* 1995; 16: 441–450.
16. Venneti S, Lopresti BJ and Wiley CA. The peripheral benzodiazepine receptor (Translocator protein 18kDa) in microglia: from pathology to imaging. *Prog Neurobiol* 2006; 80: 308–322.
17. Hashimoto K, Inoue O, Suzuki K, et al. Synthesis and evaluation of 11C-PK 11195 for in vivo study of peripheral-type benzodiazepine receptors using positron emission tomography. *Ann Nucl Med* 1989; 3: 63–71.
18. James ML, Fulton RR, Vercoullie J, et al. DPA-714, a new translocator protein-specific Ligand: Synthesis, radiofluorination, and pharmacologic characterization. *J Nucl Med* 2008; 49: 814–822.
19. Chauveau F, Van Camp N, Dollé F, et al. Comparative evaluation of the translocator protein radioligands 11C-DPA-713, 18F-DPA-714, and 11C-PK11195 in a rat model of acute neuroinflammation. *J Nucl Med* 2009; 50: 468–476.
20. Vicidomini C, Panico M, Greco A, et al. In vivo imaging and characterization of [(18)F]DPA-714, a potential new TSPO ligand, in mouse brain and peripheral tissues using small-animal PET. *Nucl Med Biol* 2015; 42: 309–316.
21. Arlicot N, Vercouillie J, Ribeiro MJ, et al. Initial evaluation in healthy humans of [18F]DPA-714, a potential PET biomarker for neuroinflammation. *Nucl Med Biol* 2012; 39: 570–578.
22. Golla SSV, Boellaard R, Oikonen V, et al. Quantification of [18F]DPA-714 binding in the human brain: initial studies in healthy controls and Alzheimer's disease patients. *J Cereb Blood Flow Metab* 2015; 35: 766–772.
23. Owen DR, Yeo AJ, Gunn RN, et al. An 18-kDa translocator protein (TSPO) polymorphism explains differences in binding affinity of the PET radioligand PBR28. *J Cereb Blood Flow Metab* 2012; 32: 1–5.
24. Dodart JC, Mathis C, Bales KR, et al. Does my mouse have Alzheimer's disease? *Genes Brain Behav* 2002; 1: 142–155.
25. Hamacher K, Coenen HH and Stöcklin G. Efficient stereospecific synthesis of no-carrier-added 2-[18F]-fluoro-2-deoxy-D-glucose using aminopolyether supported nucleophilic substitution. *J Nucl Med* 1986; 27: 235–238.
26. Radde R, Bolmont T, Kaeser SA, et al. Abeta42-driven cerebral amyloidosis in transgenic mice reveals early and robust pathology. *EMBO* 2006; 7: 940–946.
27. Rupp NJ, Wegenast-Braun BM, Radde R, et al. Early onset amyloid lesions lead to severe neuritic abnormalities and local, but not global neuron loss in APPPS1 transgenic mice. *Neurobiol Aging* 2011; 32: 2324.e1–2324.e6.
28. Mouse MRI brain template. MRM NAt Mouse Brain Database, McKnight Brain Institute, http://brainatlas.mbi.ufl.edu/Database/ (2005, accessed 17 May 2013).
29. De Leon MJ, George AE, Ferris SH, et al. Regional correlation of PET and CT in senile dementia of the Alzheimer type. *AJNR Am J Neuroradiol* 1983; 4: 553–556.
30. Friedland RP, Budinger TF, Ganz E, et al. Regional cerebral metabolic alterations in dementia of the Alzheimer type: positron emission tomography with

[18F]fluorodeoxyglucose. *J Comput Assist Tomogr* 1983; 7: 590–598.
31. Deleye S, Waldron AM, Richardson JC, et al. The effects of physiological and methodological determinants on 18F-FDG mouse brain imaging exemplified in a double transgenic Alzheimer model. *Mol Imaging* 2016; 15: 1–11.
32. Foster NL, Wang AY, Tasdizen T, et al. Realizing the potential of positron emission tomography with 18F-fluorodeoxyglucose to improve the treatment of Alzheimer's disease. *Alzheimers Dement* 2008; 4: S29–S36.
33. Herholz K, Carter SF and Jones M. Positron emission tomography imaging in dementia. *Br J Radiol* 2007; 80: S160–S167.
34. Aso E, Lomoio S, López-González I, et al. Amyloid generation and dysfunctional immunoproteasome activation with disease progression in animal model of familial Alzheimer's disease. *Brain Pathol* 2012; 22: 636–653.
35. Hiltunen M, Khandelwal VK, Yaluri N, et al. Contribution of genetic and dietary insulin resistance to Alzheimer phenotype in APP/PS1 transgenic mice. *J Cell Mol Med* 2012; 16: 1206–1222.
36. Pedrós I, Petrov D, Allgaier M, et al. Early alterations in energy metabolism in the hippocampus of APPswe/PS1dE9 mouse model of Alzheimer's disease. *Biochim Biophys Acta* 2014; 1842: 1556–1566.
37. Rojas S, Herance JR, Gispert JD, et al. In vivo evaluation of amyloid deposition and brain glucose metabolism of 5XFAD mice using positron emission tomography. *Neurobiol Aging* 2013; 34: 1790–1798.
38. Macdonald IR, DeBay DR, Reid GA, et al. Early detection of cerebral glucose uptake changes in the 5XFAD mouse. *Curr Alzheimer Res* 2014; 11: 450–460.
39. Liu B, Le KX, Park MA, et al. In vivo detection of age- and disease-related increases in neuroinflammation by 18F-GE180 TSPO microPET imaging in wild-type and Alzheimer's transgenic mice. *J Neurosci* 2015; 35: 15716–15730.
40. Prokop S, Miller KR and Heppner FL. Microglia actions in Alzheimer's disease. *Acta Neuropathol* 2013; 126: 461–477.
41. Venneti S, Lopresti BJ, Wang G, et al. PK11195 labels activated microglia in Alzheimer's disease and in vivo in a mouse model using PET. *Neurobiol Aging* 2009; 30: 1217–1226.
42. Rapic S, Backes H, Viel T, et al. Imaging microglial activation and glucose consumption in a mouse model of Alzheimer's disease. *Neurobiol Aging* 2013; 34: 351–354.
43. Mirzaei N, Tang SP, Ashworth S, et al. In vivo imaging of microglial activation by positron emission tomography with [(11) C]PBR28 in the 5XFAD model of Alzheimer's disease. *Glia* 2016; 64: 993–1006.
44. James ML, Belichenko NP, Nguyen TVV, et al. Pet imaging of translocator protein (18 kDa) in a mouse model of Alzheimer's disease using N-(2,5,dimethoxybenzyl)-2-18F-fluoro-N-(2-phenoxyphenyl)acetamide. *J Nucl Med* 2015; 56: 311–316.
45. Sérrière S, Tauber C, Vercouillie J, et al. Amyloid load and translocator protein 18 kDa in APPswePS1-dE9 mice: a longitudinal study. *Neurobiol Aging* 2015; 36: 1639–1652.
46. Tan J, Town T, Paris D, et al. Microglial activation resulting from CD40-CD40L interaction after beta-amyloid stimulation. *Science* 1999; 286: 2352–2355.
47. Herber DL, Roth LM, Wilson D, et al. Time-dependent reduction in Abeta levels after intracranial LPS administration in APP transgenic mice. *Exp Neurol* 2004; 190: 245–253.
48. Guillot-Sestier MV, Doty KR and Town T. Innate immunity fights Alzheimer's disease. *Trends Neurosci* 2015; 38: 674–681.
49. Krabbe G, Halle A, Matyash V, et al. Functional impairment of microglia coincides with Beta-amyloid deposition in mice with Alzheimer-like pathology. *PLoS One* 2013; 8: e60921.
50. Heneka MT, O'Banion MK, Terwel D, et al. Neuroinflammatory processes in Alzheimer's disease. *J Neural Transm* 2010; 117: 919–947.
51. Thie JA. Understanding the standardized uptake value, its methods, and implications for usage. *J Nucl Med* 2004; 45: 1431–1434.
52. Lyoo CH, Ikawa M, Liow JS, et al. Cerebellum can serve as a pseudo-reference region in Alzheimer disease to detect neuroinflammation measured with PET radioligand binding to translocator protein. *J Nucl Med* 2015; 56: 701–706.
53. Brendel M, Probst F, Jaworska A, et al. Glial activation and glucose metabolism in a transgenic amyloid mouse model: A triple tracer PET study. *J Nucl Med* 2016; 57: 954–960.
54. Kleiber M. Body size and metabolic rate. In: Kleiber M (ed.) *The fire of life – An Introduction to Animal Energetics*. Huntington, NY: Robert E. Krieger Publishing Company, 1975, pp.179–222.
55. Schmidt-Nielsen K. Metabolic rate and body size. In: Schmidt-Nielsen K(ed.) *Scaling: Why is animal size so important?* Cambridge: Cambridge University Press, 1984, pp.56–77.
56. Gordon JC. *Temperature regulation in laboratory rodents*. New York, USA: Cambridge University Press, 1993.
57. Fueger BJ, Czernin J, Hildebrandt I, et al. Impact of animal handling on the results of 18F-FDG PET studies in mice. *J Nucl Med* 2006; 47: 999–1006.
58. Toyama H, Ichisea M, Liowa JS, et al. Evaluation of anesthesia effects on [18F]FDG uptake in mouse brain and heart using small animal PET. *Nucl Med Biol* 2004; 31: 251–256.
59. Claassen V. *Neglected factors in pharmacology and neuroscience research: Biopharmaceutics, animal characteristics, maintanance, testing conditions*. Amsterdam: Elsevier Science, 1994.
60. Wingfield JC and Kitaysky AS. Endocrine responses to unpredictable environmental events: Stress or anti-stress hormones? *Integr Comp Biol* 2002; 42: 600–609.
61. Reiman EM, Uecker A, Gonzalez-Lima F, et al. Tracking Alzheimer's disease in transgenic mice using fluorodeoxyglucose autoradiography. *Neuroreport* 2000; 11: 987–991.